Electronic Supplementary Material (ESI) for Catalysis Science & Technology.

Supplementary Information

Role of metal (Pt)–support (MgO) interactions in the base-free glucose dehydrogenation

Jiaxin Liu, Chuang Li, Hongyu Niu and Changhai Liang*

Laboratory of Advanced Materials and Catalytic Engineering, School of Chemical Engineering, Dalian University of Technology, 2 Linggong Road, Dalian 116024, P. R. China

Table S1 Dehydrogenation of glucose on different catalysts

Catalyst	Conversion（%）	H_2 Yield（%）	GNA Yield（%）
3 Pt/TiO_2	2.1	Trade	1.7
3 Pt/Al_2O_3	0	0	0
3 Pt/CeO_2	6.6	5.1	6.2
3 Pt/CNTs	0	0	0
3 Pt/MgO[a]	17.5	15.7	16.1
3 Pt/CNTs + MgO[b]	8.9	7.5	7.9
3 Pt/CNTs + KOH[c]	12.6	10.4	11.1
2.5 Pt/CNTs + KOH[d]	9.6	8.1	8.5

Reaction conditions: 30 °C; 110 min; catalyst: 0.15 g; 0.03 mol mL^{-1} glucose solution (30 mL methanol + 10 mL H_2O)

The pH of a-d reaction system was consistent (pH = 10).

$TOF^a = 0.15\ min^{-1}$

$TOF^b = 0.08\ min^{-1}$

$TOF^c = 0.11\ min^{-1}$

$TOF^d = 0.09\ min^{-1}$

In the catalytic oxidation of glucose, the intrinsic reaction rate or turnover frequency (TOF; min^{-1}) can be expressed as

$TOF = r/n$

where n is the number of active sites (according to CO chemisorption) and r is the reaction rate (the average reaction rate over 110 min, where the reaction rate is in the kinetic range and the effect of diffusion is disregarded).

Methanol is frequently used as a solvent in catalytic biomass conversion because it modifies the free energies of material surfaces and liquid-phase species via solvation and increases the product yield.[1,2]

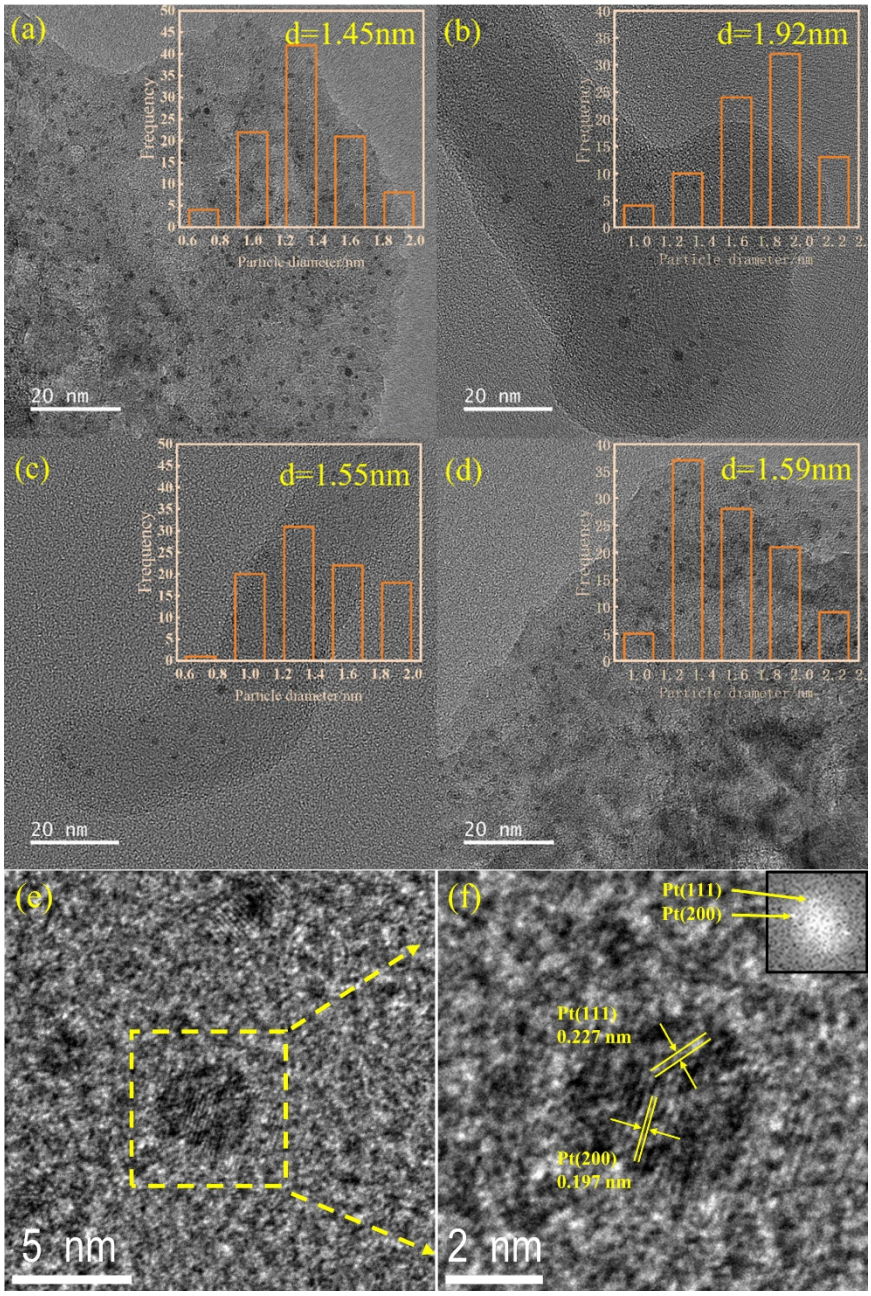

Figure S1 Particle size distributions and TEM images: (a) 3 Pt/MgO; (b) 3 Pt/CNTs; (c) 2.5 Pt/CNTs; (d) 3 Pt/MgO after reaction; (e, f) HRTEM images of the 3 Pt/MgO.

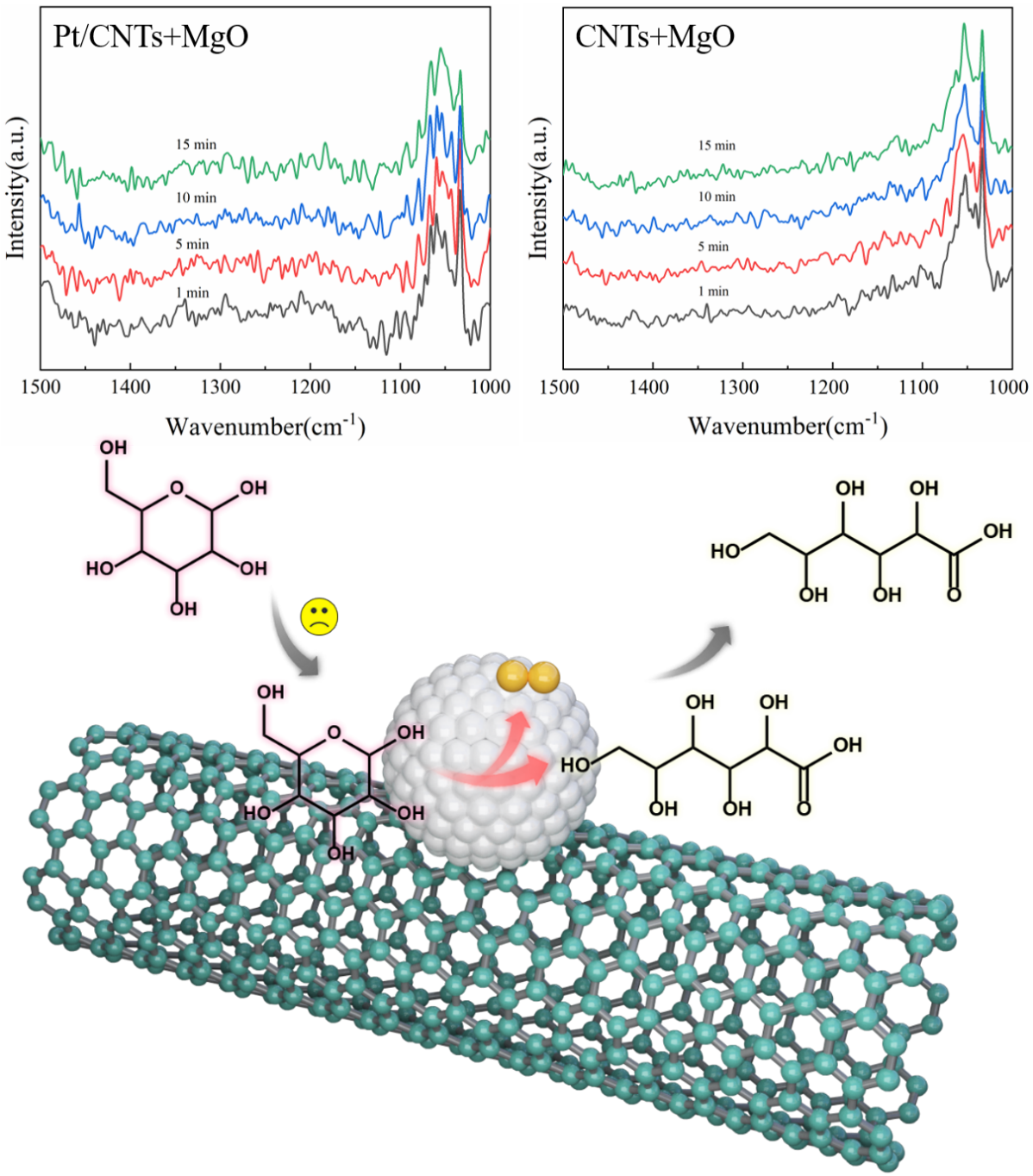

Figure S2 Fourier-transformed infrared spectra of glucose adsorption on Pt/CNTs + MgO and CNTs + MgO samples and schematic diagram of glucose dehydrogenation process on Pt/CNTs.

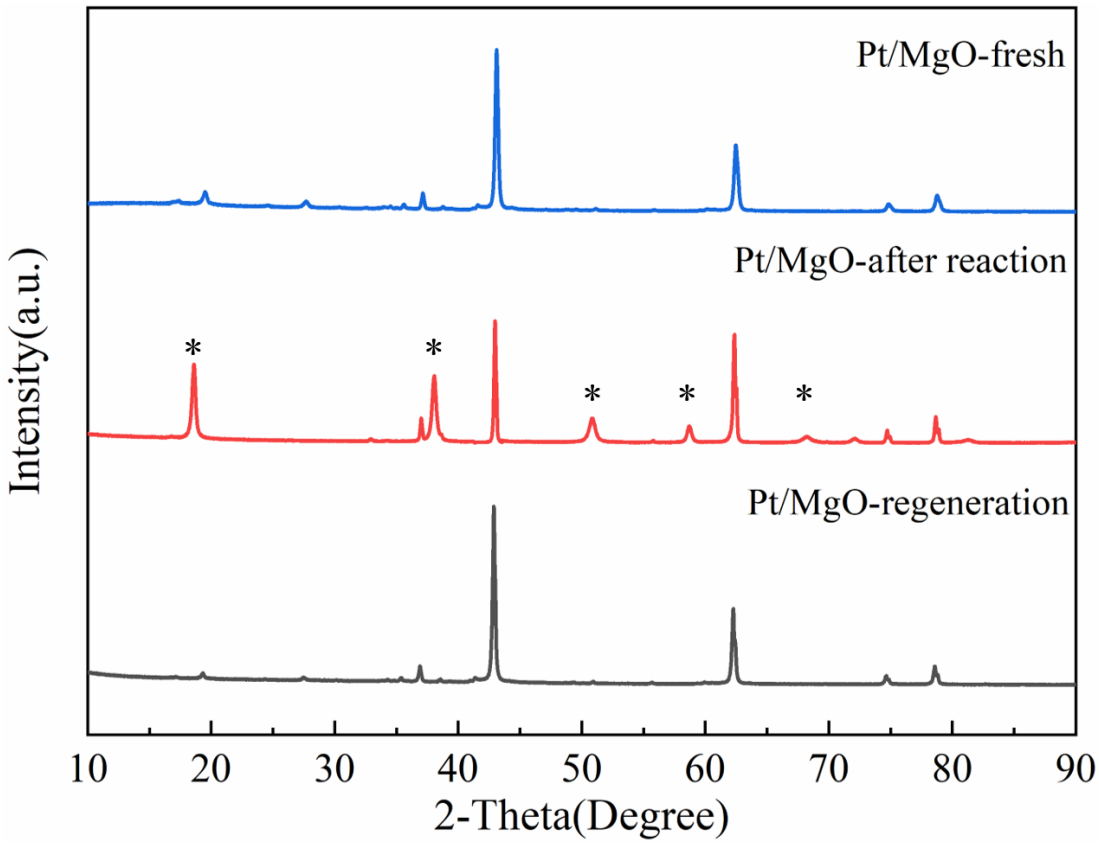

Figure S3 XRD patterns of Pt/MgO catalysts (* peaks corresponding to $Mg(OH)_2$).

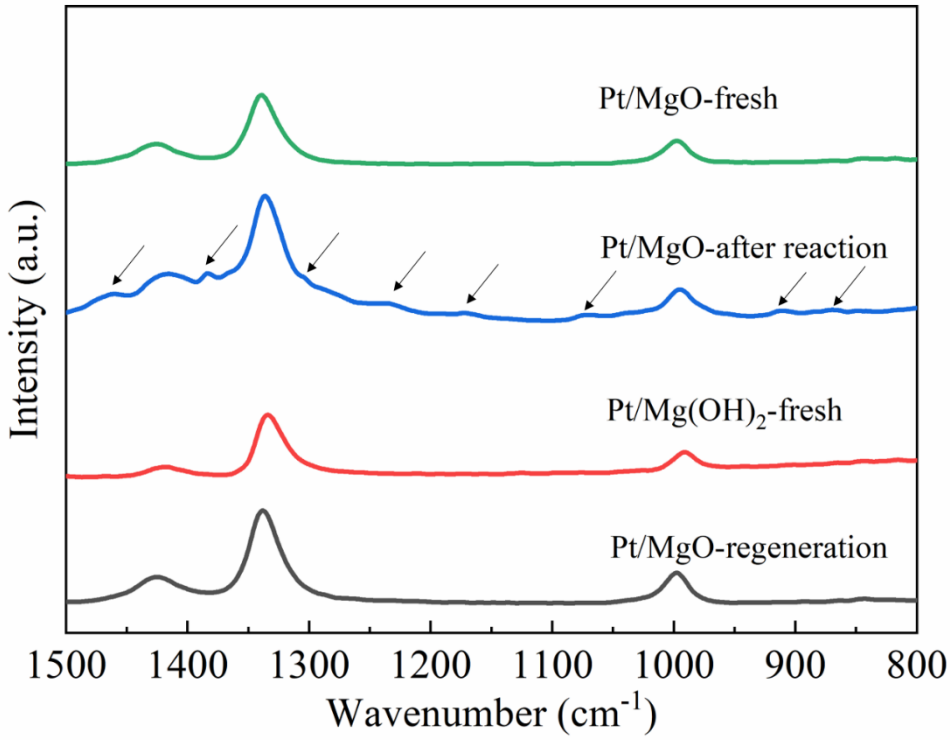

Figure S4 ATR-FTIR spectra of Pt/MgO and Pt/$Mg(OH)_2$ catalysts (Arrows indicate bands associated with adsorbed organic species).

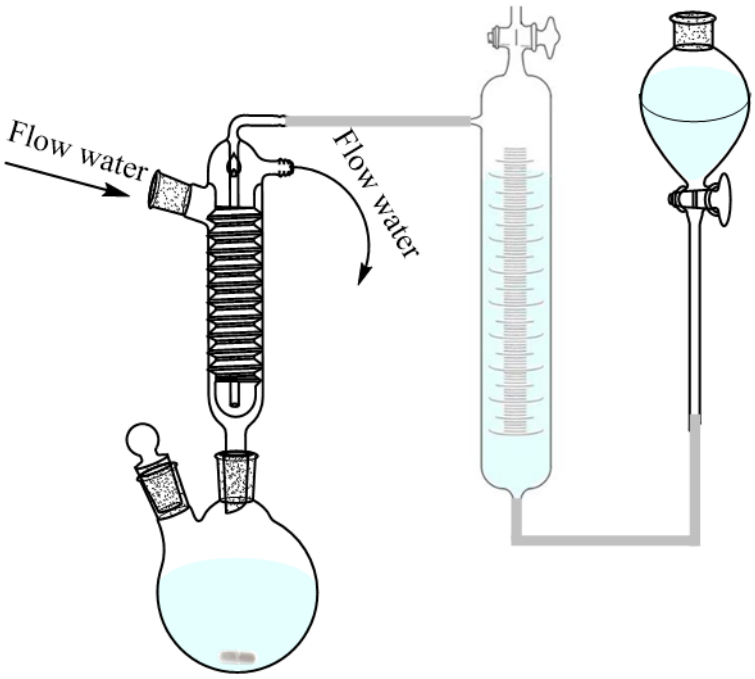

Figure S5. Schematic of the experiment set-up for glucose dehydrogenation.

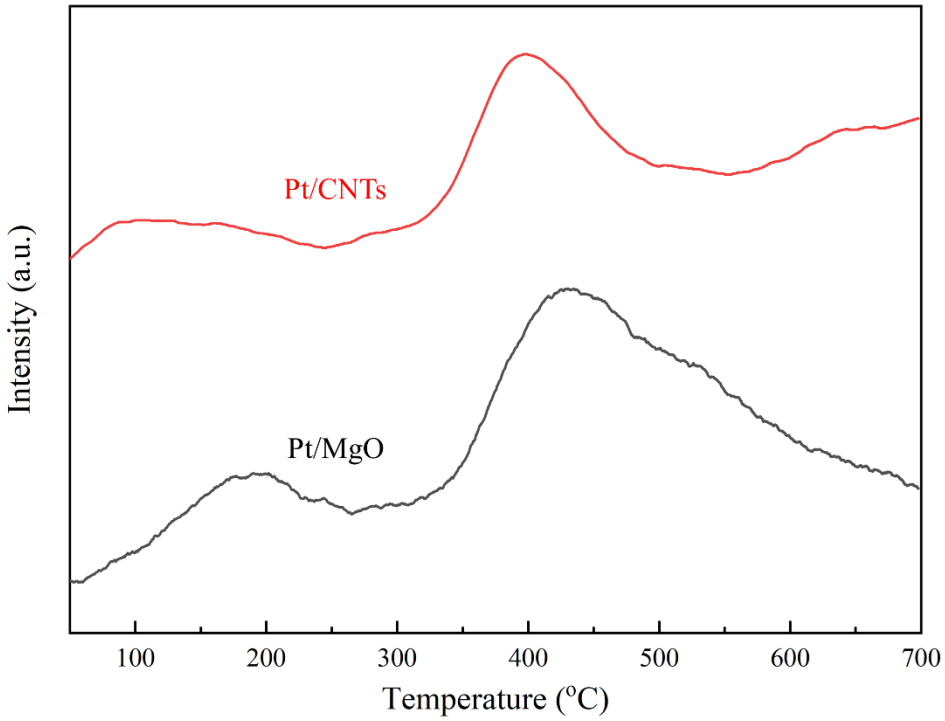

Figure S6. H_2-TPD of Pt/CNTs and Pt/MgO.

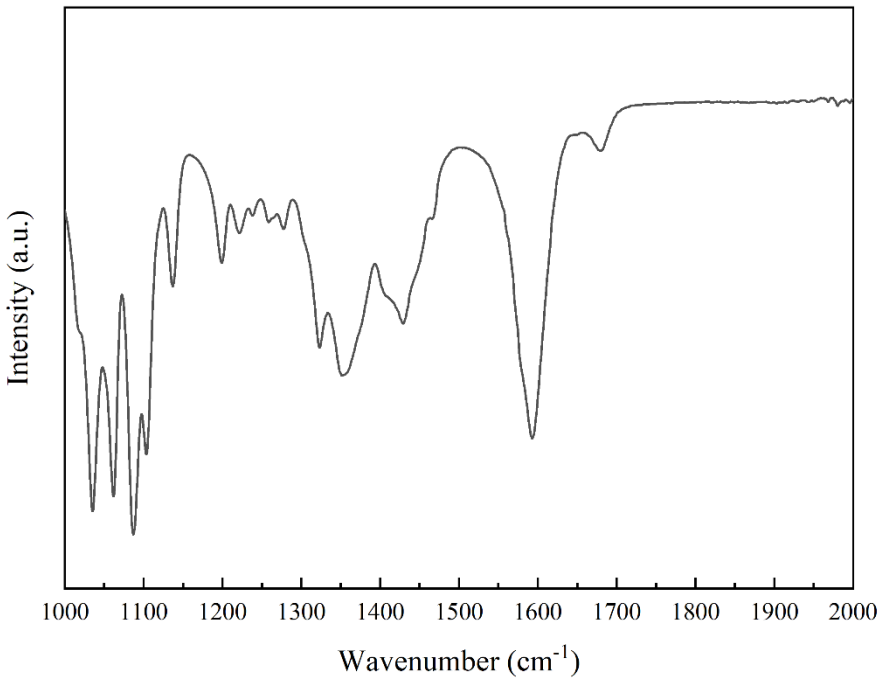

Figure S7. FTIR spectra of the liquid product.

Table S2 Band assignment of the FTIR spectra.

Wavenumber (cm^{-1})	Assignment
1550–1650	C=O stretching in COOH
1397–1341	C-H bending in $-CH_2$
1283–1250	C-H bending in CH
1050–1150	C-O stretching in CH-OH
1102–1082	C-O stretching in CH_2-OH

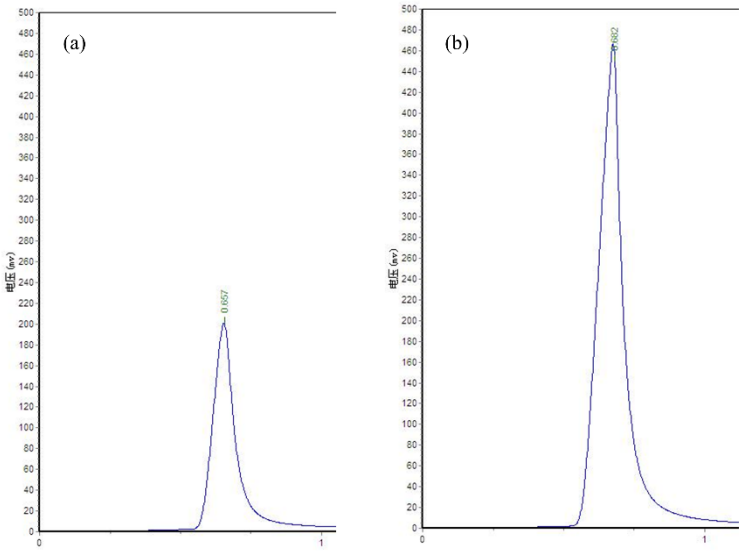

Figure S8. GC analysis of the evolved gas from the reaction of glucose catalysed under optimal conditions. (a) Chromatogram of the evolved gas; (b) Chromatogram of the standard hydrogen gas.

Table S3 Comparison of this work with other catalysts for glucose dehydrogenation.

Catalyst	Temperature (℃)	Reaction Time (h)	Additives	GNA Yield (%)	Ref.
Ir complex[a]	110	24	H_2SO_4	~97	3
Ir complex[b]	110	20	-	~100	4
Ir complex[c]	110	20	-	~95	5
Pt/MgO	30	2	-	~16	This work

a Iridium (III) complexes containing the fragment $[Cp^*Ir(NHC)]^{2+}$

b Iridium (III) complexes containing the fragment $Cp^*Ir(carbene)Cl_2$

c Iridium (III) complexes containing the fragment $[Cp^*Ir(6,60\text{-dihydroxy-}2,20\text{-bipyridine})(H_2O)][OTf]_2$

Cp*: pentamethylcyclopentadienyl, NHC: N-heterocyclic carbene ligand, OTf: trifluoromethanesulfonate

The research on glucose dehydrogenation currently focuses on the use of iridium complexes as catalysts. The mainstream research direction is to be additive-free. Compared with the existing research, the use of heterogeneous catalysts in this study is more promising for future applications.

References

[1] D. S. Potts, D. T. Bregante, J. S. Adams, C. Torres, D. W. Flaherty, *Chem. Soc. Rev.*, 2021, **50**, 12308-12337.

[2] M. A. Mellmer, C. Sanpitakseree, B. Demir, P. Bai, K. Ma, M. Neurock, J. A. Dumesic, *Nat. Catal.*, 2018, **1**, 199-207.

[3] P. Borja, C. Vicent, M. Baya, H. García, J. A. Mata, *Green Chem.*, 2018, **20**, 4094-4101.

[4] A. Mollar‐Cuni, J. P. Byrne, P. Borja, C. Vicent, M. Albrecht, J. A. Mata, *ChemCatChem*, 2020, **12**, 3746-3752.

[5] K. Fujita, T. Inoue, T. Tanaka, J. Jeong, S. Furukawa, R. Yamaguchi, *Catalysts*, 2021, **11**, 891-899.

Cartesian coordinates of the optimized structures

Fig. 3c

C	0.96316	1.00575	0.38813
C	1.61293	−0.10378	−0.42298
C	1.02488	−1.46595	−0.0674
C	−1.02923	−0.45716	0.56618
C	−0.53544	0.94548	0.20584
H	1.37703	−2.23971	−0.76105
H	1.38792	0.07992	−1.48366
H	1.19925	0.8466	1.45438
H	−0.78217	−0.65489	1.61922
H	−0.7674	1.14154	−0.85008
O	−1.14227	1.92014	1.04211
H	−2.01757	2.09085	0.68199
O	1.44809	2.26482	−0.04316
H	2.40372	2.15129	−0.11235
O	3.00797	−0.00172	−0.18333
H	3.47112	−0.43105	−0.90758
O	1.38161	−1.76468	1.25348
H	1.10193	−2.6684	1.43074

O	−0.37863	−1.43467	−0.26064
C	−2.51929	−0.61259	0.40144
H	−2.77419	−1.67639	0.49343
H	−3.01498	−0.07886	1.2241
O	−2.90388	−0.08608	−0.85931
H	−3.85724	−0.17641	−0.9305
Pt	−1.65275	−1.34854	−2.16906

Fig.3d

C	0.96316	1.00575	0.38813
C	1.61293	−0.10378	−0.42298
C	1.02488	−1.46595	−0.0674
C	−1.02923	−0.45716	0.56618
C	−0.53544	0.94548	0.20584
H	1.37703	−2.23971	−0.76105
H	1.38792	0.07992	−1.48366
H	1.19925	0.8466	1.45438
H	−0.78217	−0.65489	1.61922
H	−0.7674	1.14154	−0.85008
O	−1.14227	1.92014	1.04211
H	−2.01757	2.09085	0.68199

O	1.44809	2.26482	−0.04316
H	2.40372	2.15129	−0.11235
O	3.00797	−0.00172	−0.18333
H	3.47112	−0.43105	−0.90758
O	1.38161	−1.76468	1.25348
H	1.10193	−2.6684	1.43074
O	−0.37863	−1.43467	−0.26064
C	−2.51929	−0.61259	0.40144
H	−2.77419	−1.67639	0.49343
H	−3.01498	−0.07886	1.2241
O	−2.90388	−0.08608	−0.85931
H	−3.85724	−0.17641	−0.9305
Pt	−1.65275	−1.34854	−2.16906